

Synergetic Surface and Chemical Durability Study of the Aesthetically Enhanced Natural Quartz by Heat Treatment



RAKESH K. SAHOO, PRAJNA P. ROUT, SAROJ K. SINGH, BARADA K. MISHRA,
and BIRENDRA K. MOHAPATRA

The change in surface behavior of natural quartz stone before and after heat treatment with metal oxides such as: cobalt oxide (Co_3O_4) and copper oxide (Cu_2O) under vacuum and open atmosphere has been investigated. The surface feature, bulk density and hardness value of quartz changed after heat treatment, converting to a high value product. Difference in crystallinity of quartz, pre- and post-heat treatment was obtained through X-ray diffraction (XRD) study. The electron probe microanalysis results clearly explicated the diffusion of metal ion in quartz matrix exposed under vacuum atmosphere but as coating on the surface under open atmosphere. The structural transformation of quartz after heat treatment has been observed from the XRD data and well corroborated with the nanoindentation results. Durability of such quartz to chemical hazardous environment was observed. Thus, this communication demonstrates the change in physical and chemical characteristics of natural quartz stone after heat treatment under different atmosphere.

DOI: 10.1007/s11661-016-3918-4

© The Minerals, Metals & Materials Society and ASM International 2017

I. INTRODUCTION

QUARTZ is one of the most abundant minerals found in Earth's crust (around 12 pct). Though quartz is chemically inert, the changes in pressure (P)–temperature (T) conditions cause variations in its crystallographic structure.^[1] The thermal luminescence property of this mineral makes it a technological material in radiation science and engineering. In dosimetry, quartz is used in testing the authenticity of art objects, nuclear accidents,^[2] food irradiation control,^[3] and dating of archeological materials and sediments.^[4–6]

Recent studies show that quartz is used in various advanced applications such as quartz cement,^[7] quartz crystal microbalance sensors,^[8] quartz crystal with transparent electrode used for localized surface plasmon resonance (SPR) sensing with quartz crystal microbalance with dissipation monitoring technology,^[9] paramagnetic lattice defects in quartz for applications to electron spin resonance dating for advance applications to fault gouge, tephra and sediment,^[10] radio fluorescence,^[11] as a sensor for detection of ammonia in human breath,^[8] photoacoustic spectroscopy,^[12] and tuning fork-based conductive atomic force microscopes with glue-free solid metallic tips.^[13]

The optical, thermal, piezoelectric properties make natural quartz an interesting material for technological and gemological applications. Defects, vacancies, and impurities, basically Al, Fe, Ti, Na, K, Zn, Ge, P, *etc.*, adversely affect all the preceding properties.^[14,15] The gemological quality of the quartz demands an attractive color and durability. The color of the natural quartz is modified using several methods such as dying, heating, irradiation, *etc.* Coloration of quartz crystals is possible through the incorporation of transition metal impurities such as V^{3+} for royal blue, Cr^{3+} for green, Ni^{3+} for green fluorescence, Cu^{2+} for yellow-green fluorescence, Co^{2+} for blue, and Fe^{3+} for amber-brown.^[16] The possibility to dope quartz by thermal diffusion is an interesting issue from both technological and scientific points of view.

In this study, we compare the aesthetic value and surface diffusion characteristics of the natural quartz by thermal diffusion of metallic ions in quartz samples, which were collected from the Nuapada district of Odisha. Quartz in two different colors, *i.e.*, light blue and pink, has a high market value and can be treated as a low-price version of the blue topaz and citrine. Hence, a simple attempt is carried out to study the change in surface color and luster of the natural quartz by heat treatment with cobalt oxide for blue and copper oxide for pink coloration. X-ray diffraction (XRD) and Raman spectroscopic studies were conducted to determine the change in phase and structures of the samples after diffusion, whereas the color appearance and presence of color centers and absorption due to the impurity ions are analyzed using UV–Vis–DRS spectroscopy. The change in the surface profile of the diffusing cobalt ions in different heating environments was analyzed using electron probe microanalysis (EPMA). The gemological

RAKESH K. SAHOO, SAROJ K. SINGH, BARADA K. MISHRA, and BIRENDRA K. MOHAPATRA are with the CSIR - Institute of Minerals and Materials Technology, Bhubaneswar 751013, India. Contact email: rakesh.materialscience@gmail.com PRAJNA P. ROUT, formerly with the CSIR - Institute of Minerals and Materials Technology, is now with the Department of Physics, Government Polytechnic, Moto, Puri, Odisha 752011, India.

Manuscript submitted April 22, 2016.

Article published online January 17, 2017

parameters, such as specific gravity and nanoindentation value of these quartz stones before and after heat treatment, were obtained and the enhancement in the hardness values explicated. The durability of the treated stones is tested in 0.1N HCl solution for different times. Moreover, in this work, the effect of heating atmosphere in the phase formation, optical and vibrational transition, specific gravity, and hardness of the material was analyzed, and its synergetic change in aesthetic value (color, clarity, and durability) improvement was elucidated.

II. MATERIALS METHODS

The quartz sample in crystalline form was collected from pegmatite vein traversing nepheline syenite in Khariar, Nuapada district, Odisha, India).

A. Surface Treatment of the As-Received Quartz

The quartz stones were surface cleaned with acetone, dilute HCl, and subsequently by HF to remove the interface and inherent impurities present in them. The alumina crucible containing quartz covered with Co_3O_4 powder was loaded into a resistance-heated muffle furnace (Model No. TQ1164, Relek Pvt. Ltd.). The sample was then heated in an open atmosphere to 773.15 K (500 °C) with a heating rate of 283.15 K (10 °C/min). After 773.15 K (500 °C), the system was ramped up to 1473.15 K (1200 °C) in the same atmosphere with a heating rate of 281.15 K/min (8 °C/min). Thereafter, the system was kept for 2 hours in 1473.15 K (1200 °C) in the same atmosphere. Finally, the reactor temperature was turned off and the system was cooled to room temperature. A similar procedure was also adopted for the Cu_2O treatment. However, for the vacuum-treated sample, the sample was placed in a resistance-heated vacuum furnace (VICO (VF-2000)). First, the sample covered with Co_3O_4 powder was gently pressed into pellet form and then placed inside the vacuum furnace. Then the system was pumped down to 10^{-6} torr and, subsequently, ramped up to 1473.15 K (1200 °C) with a heating rate of 281.15 K/min (8 °C/min) and left at that temperature for 2 hours. After placing the sample in the required temperature and time, the system was cooled to room temperature in the same vacuum condition.

B. Characterization of the Materials

The true density was determined by using water and was calculated from the following empirical formula:

$$\text{True density (g/cm}^3\text{)} = W_1 / (W_1 - W_2)$$

where W_1 is the weight of the solid body in air and W_2 is the weight of the solid body when immersed in water.

A field emission scanning electron microscope (Oxford, Zeiss SUPRA* 40) equipped with an

energy-dispersive X-ray analyzer (Oxford Instruments) was employed for examination of the morphology and microstructure of the quartz samples. Phase and structural analysis of the samples were carried out by an X-ray diffractometer (Regaku Ultimatev) using Cu K_α source. Diffused reflective spectroscopy UV-Vis (DRS-UV-Vis) study was adopted to observe the absorption wavelength of the quartz before and after surface treatment. A Varian Cary UV-Vis spectrophotometer equipped with a diffuse reflectance accessory in the region 200 to 800 nm with an integrating sphere of 150 mm was used for the measurement. Micro Raman measurements were carried out at room temperature using a Seki Technotron Corp. (STR250) instrument in a backscattering geometry. An Ar-Kr ion laser with 514-nm wavelength was used as an excitation source. The Raman spectrometer was equipped with a double subtractive monochromator with an 1800 grooves/mm holographic grating and a Peltier-cooled CCD detector. An electron probe microstructure analyzer (EPMA) (Model No. JXA-8100, JEOL**) was used to study the

**JEOL is a trademark of Japan Electron Optics Ltd., Tokyo.

cobalt oxide-diffused quartz samples. Trace impurities in the natural quartz were analyzed using inductively coupled plasma-optical emission spectrometry (ICP-OES) Perkin Elmer Optima 2100 DV system. Finally, the weight loss of the samples in the acid environment was analyzed using a Citizen CX-265 digital balance for the durability study. The hardness of the materials was analyzed using a UMIS nanoindentation system (Frischer-Cripps, New South Wales, Australia). A Berkovich indenter with a face angle of 65.3 deg and tip radius of 150 nm was employed for the nanoindentation measurements.

III. RESULTS AND DISCUSSION

A. Visual Characteristics

To understand the complete process and outcome of this study, very simply and distinctively, the schematic color presentation was done. The color of the stones before and after heat treatment with additives is schematically shown in Figure 1(a). The untreated quartz with yellow tints is shown in Figure 1(b). This stone was cut into several pieces and these stone pieces were heat treated without any additives at 1473.15 K (1200 °C), and the color changed to transparent white (Figure 1(c)). The yellow tints almost faded away. Some of the cut pieces were then covered with Co_3O_4 powder and heat treated in a vacuum atmosphere at 1473.15 K (1200 °C) for 2 hours. The color of the quartz drastically changed to royal blue with the fracture planes showing more deep color (Figure 1(d)). Treating other cut pieces of samples in two separate batches at 1473.15 K (1200 °C) in open air, surrounded with Co_3O_4 and Cu_2O powder, the color changed to deep sky blue (Figure 1(e))

*SUPRA is a trademark of Carl Zeiss AG, Oberkochen, Germany.

and maroon (Figure 1(f)), respectively. Hence, it is inferred that the heat treatment surrounding the metal oxide at high temperature enhances the overall color of the gem stone.

B. Inductively Coupled Plasma Optical Emission Spectrometry Analysis

The main chemical bulk concentrations of these quartz materials are as follows: SiO_2 (96.73 pct), FeO (1.56 pct), CaO (0.08 pct), MgO (0.09 pct), Na_2O (0.15 pct), K_2O (0.18 pct), and ZnO (0.08 pct). Additionally, some trace elements, such as Al (420 ppm) and Ti (50 ppm), are also observed.

C. Density Measurement

The true densities of the raw, heat-treated Co_3O_4 powder vacuum treated, Co_3O_4 powder treated in open air, and Cu_2O powder-treated quartz samples were measured by simple Archimedes' principle. It was found that the density values of the quartz samples after heat treatment without oxide additive indicate minute increases, whereas the density value is maximum for copper oxide-treated sample. Further, after heat

treatment with cobalt oxide in vacuum and open atmosphere, the density value also changes. Different density values are shown in Table I.

D. Phase Determination

The XRD patterns of original and treated samples are shown in Figure 2. The diffraction pattern of As-received quartz (QZ-1 shown in Figure 2(a)) matches with the $P3221$ space group symmetry of the SiO_2 (PDF No. 78-1254), and the humplike shape of the background indicates low crystallinity of the quartz sample. After heat treatment, without metal oxide additives (QZ-2), the background became flat, indicating the induction of crystallinity after heat treatment (Figure 2(b)). However, heat treatment with metal oxide additives shows a phase change on the quartz surface. After heat treatment with Co_3O_4 in vacuum (QZ-3), the XRD pattern shows two phases (Figure 2(c)): one major cubic phase of Co_2SiO_4 (PDF No. 29-0506) with $Fd-3m$ space group symmetry and the other minor phase of SiO_2 (PDF No. 29-0085). However, when the stone is treated with Co_3O_4 in open atmosphere, only the Co_2SiO_4 phase (PDF No. 15-0497) is observed on the surface (QZ-4 shown in Figure 2(d)). In the case of the Cu_2O -treated sample (QZ-5 shown in Figure 2(e)), two phases are also

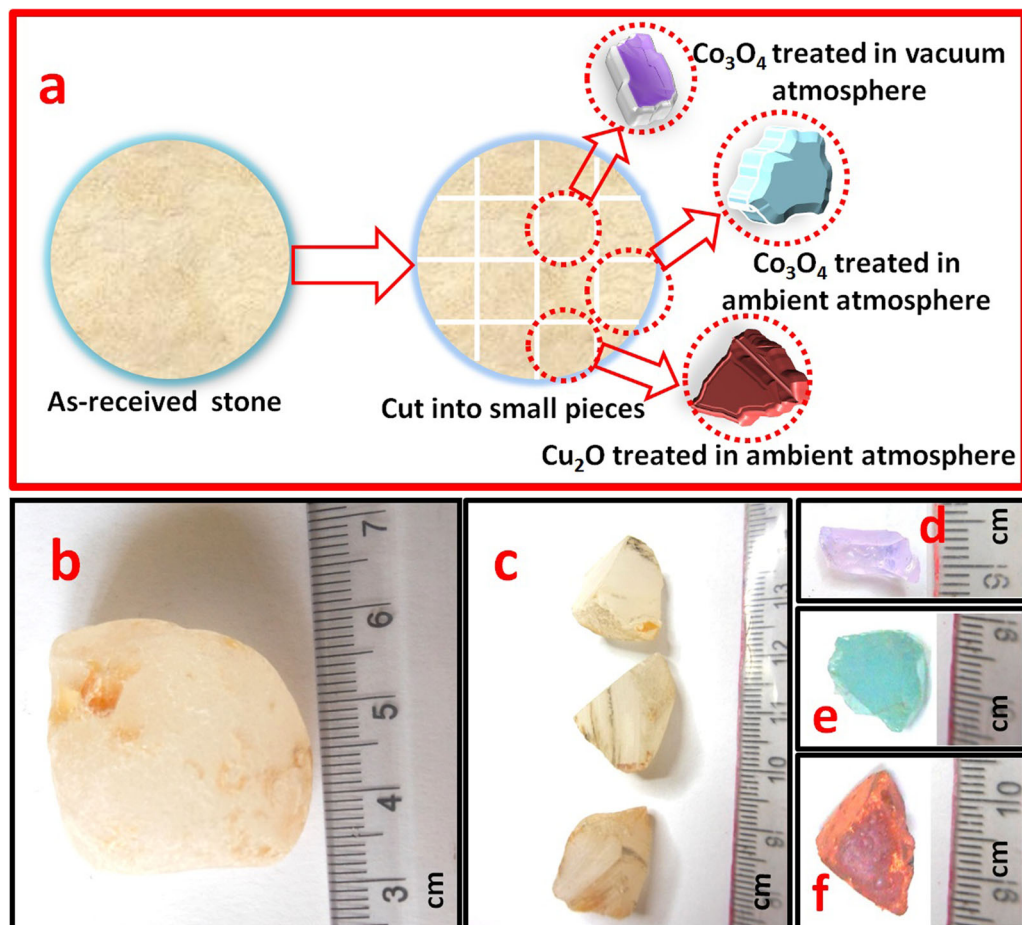


Fig. 1—Visual image of natural quartz sample: (a) schematic diagram of the complete process; (b) As-received quartz, (c) cut into small pieces, (d) after Co_3O_4 treatment in vacuum, (e) after Cu_2O treatment, and (f) after Co_3O_4 treatment in open atmosphere at high temperature.

Table I. Experimental Specification of Samples

Sample Name	Environment Condition	Temperature in K (°C)	Additive Used	Color After Heat Treatment	Specific Gravity (g/cm ³)
QZ-1	—	—	—	colorless with yellow tints	2.86
QZ-2	ambient	1473.15 (1200)	—	colorless transparent	2.85
QZ-3	vacuum (10 ⁻⁶ torr)	1473.15 (1200)	Co ₃ O ₄ powder	light blue	3.01
QZ-4	ambient	1473.15 (1200)	Co ₃ O ₄ powder	green	3.1
QZ-5	ambient	1473.15 (1200)	Cu ₂ O powder	copper red	3.21

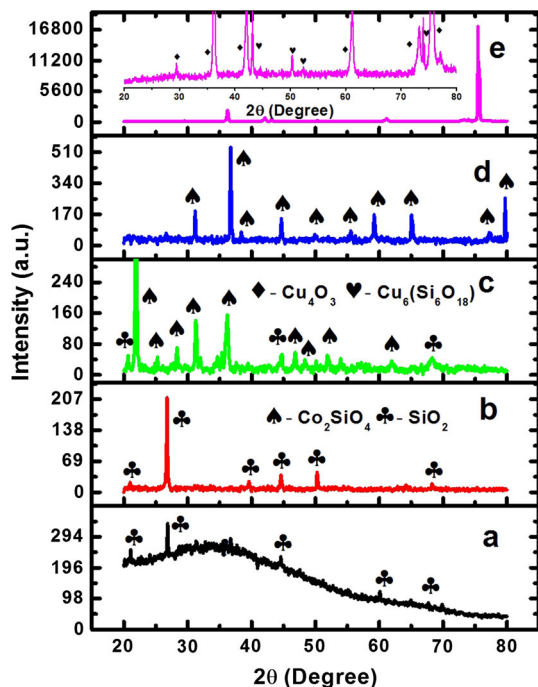


Fig. 2—XRD patterns of the natural quartz sample before and after heat treatment: (a) As received, (b) heat treated without additive, (c) with Co₃O₄ in vacuum, (d) with Co₃O₄ treatment in open atmosphere, and (e) with Cu₂O treatment in open atmosphere.

observed: one major tetragonal phase of Cu₄O₃ (PDF No. 83-1665) with *I41/amd* space group symmetry and the other secondary phase of Cu₆Si₆O₁₈ (PDF No. 79-0988) with *R-3* space group symmetry of rhombohedral structure. The most intense peak of Cu₄O₃ is supposed to appear at 35.64; however, in the present case, the most intense peak of this phase is observed at 75.4 deg, which indicates the texturing of the oxide phase along the $\langle 422 \rangle$ direction on the surface of the quartz. It is inferred that, during thermal treatment at high temperature with copper oxide, the surface diffusion of the Cu ions forms copper silicide with rhombohedral structure. This rhombohedral silicide structure induces the formation of highly crystalline tetragonal textured Cu₄O₃ layer during cooldown processes.^[17–20] This reveals that, after copper oxide treatment, the quartz phase changed with the formation of copper silicide and highly crystalline copper oxide phases. Also, heat treatment with Co₃O₄ in both vacuum and open atmosphere phase change occurs, but the crystallinity of these phases is not to the same order as that of the copper oxide-treated samples.

E. Raman Analysis

The Raman spectra of samples before and after heat treatment in the 150 to 1200 cm⁻¹ region are displayed in Figure 3. In the case of the acid cleaned sample, two low intense peaks are observed at 194 and 462 cm⁻¹. Both peaks are the signature peak of α -quartz. After heat treatment without any of the additives (QZ-2), the background of the spectrum appeared flat and some additional Raman bands were activated; also, a series of Raman peaks were observed at 201, 260, 349, 393, 461, 690, 794, and 1158 cm⁻¹. The Raman peaks observed at 201 and 260 cm⁻¹ with other low-intensity peaks are simply described as lattice vibrations.^[21] The most intense Raman peak at 461 cm⁻¹ is assigned to the A₁ phonon mode of the α -quartz, which is generated by the Si-O-Si bending modes (ν_1). The Raman peaks observed at 690, 794, and 1158 cm⁻¹ are assigned to the Si-O-Si symmetrical bending vibration (ν_4), Si-O symmetrical stretching (ν_1), and Si-O asymmetrical stretching (ν_3), respectively.

After heat treatment with Co₃O₄ additive in vacuum atmosphere (QZ-3), the Raman active peaks of the quartz are observed exactly at the same position as that of QZ-2. Magnifying the spectrum in 500 to 900 cm⁻¹ region, some additional Raman peak at 598 and 859 cm⁻¹ position is observed (Figure 3b). These two peaks are attributed to the Co-rich spinel structure and assigned as the B_{1g} asymmetric stretching (ν_4).^[22] Similar spectrum is observed in the QZ-4 sample and magnifying the spectrum in the range of 500 to 900 cm⁻¹ the B_{1g} Raman active mode is observed at 598 cm⁻¹ (Figure 3c). However, in the case of copper oxide-treated sample (QZ-5), the Raman active peaks are observed at 477, 519, 621, and 691 cm⁻¹. The Raman peaks at 477, 519, and 621 cm⁻¹ are aroused from the E_g, A_{1g}, and B_{1g} Raman modes of Cu₄O₃,^[24] where the most intense peak at 691 cm⁻¹ is assigned to the overtone of Cu₆Si₆O₁₈ and the A_g fundamental mode represents the O₁ breathing mode.^[25] Thus, the Raman analysis confirmed the presence of both Co₂SiO₄ and SiO₂ phase after heat treatment with Co₃O₄ in both vacuum and open atmosphere. However, in the case of copper oxide-treated sample, two copper-associated phases, *i.e.*, Cu₄O₃ and Cu₆Si₆O₁₈, along with the SiO₂ phase, are formed. This result is in good agreement with the XRD data.

F. UV-Vis-DRS Analysis

The absorption spectra of quartz samples before and after heat treatment in the range of 200 to 800 nm are shown in Figure 4. Before treatment, the absorption

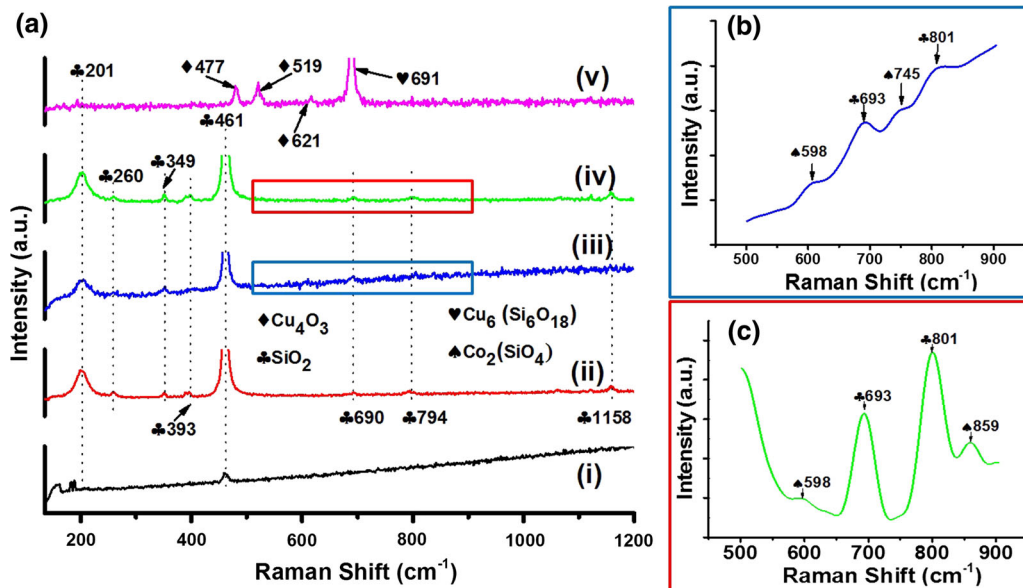


Fig. 3—Comparative Raman spectra of quartz sample before and after heat treatment: (a-i) as-received (a-ii) heat treated without additive, (a-iii) with Co_3O_4 in vacuum, (a-iv) with Co_3O_4 treatment in open atmosphere, (a-v) after Cu_2O treatment, (b) magnified view of the rectangular mark part of (a-iii) and (c) magnified view of the rectangular mark part of (a-iv).

peaks of quartz are observed at 244, 289, 319, and 487 nm and a broad shoulder at 395 nm, as shown in Figure 6(a). The strong peak at 244 nm is also observed for all other samples after heat treatment, and this band is assigned as the D_0 band, whereas the bands at 289 and 319 nm are assigned as the B_1 band. The bands at 487 nm are observed due to the Al impurities present in the sample.^[26,27] The small absorption band at 210 nm and the band at 487 nm are associated with the O^- and E' defect centers. The E' centers are basically the oxygen vacancies formed during the transformation of the oxygen tetrahedra to a planner arrangement of three oxygen ions, whereas the O^- centers represent different types of defect electrons on O^{2-} in tetrahedra with silicon vacancies. These defect centers are predominantly observed in low or noncrystalline quartz in the presence of Al and other impurities.^[28,29] The ICP-OES result (Section III-B) confirmed the presence of trace Al and other impurities in the sample.

Several interesting features are observed in the DRS spectra shown in Figure 4. First, a low absorption peak at 487 nm, which is observed for the original sample, completely vanishes. Second, the shoulder at 398 nm of the raw sample becomes activated after heat treatment (the red arrow mark is shown in Figure 4(ii) with (QZ-3) or without (QZ-2) metal oxide additives. In the case of QZ-2, the increase in the $[\text{AlO}_4]^{0-}$ defect centers after heat treatment is responsible for the enhancement of the shoulder.^[30] For QZ-3, the increase in the $[\text{AlO}_4]^{0-}$ defect centers and the absorption due to the SPR, which was generated by the diffused cobalt particles inside the silica matrix,^[30,31] together are responsible for the absorption enhancement. Third, in the case of both cobalt oxide-treated samples (in vacuum and open air), a strong broad absorption in the range of 450 to 625 nm comes basically from the

Co^{2+} absorption. This broad absorption is due to the crystal field $d-d^*$ transitions of tetrahedral coordinated Co^{2+} ions, which correspond to the ${}^4\text{A}_2(\text{F}) \rightarrow {}^2\text{A}_1(\text{G})$, ${}^4\text{A}_2(\text{F}) \rightarrow {}^4\text{T}_1(\text{P})$, and ${}^4\text{A}_2(\text{F}) \rightarrow {}^2\text{E}(\text{G})$ transitions.^[32,33] Fourth, in the case of the copper oxide-treated sample, the peak at 215 nm gained prominence and an additional peak was observed at 674 nm, indicating the absorbance of the defect centers or F centers. In general, the basic absorption of the copper ions in the silicate glass is observed above 800 nm.^[34] Thus, it is resolved that a significant number of F centers and impurity ions present in the As-received quartz stones participate in the surface coloration of the gem stones during heat treatment.

G. Hardness Measurement

The typical nanoindentation load–depth hysteresis curve for the samples before and after heat treatment is shown in Figure 5. The hardness (H) and Young's modulus (E) of the samples (natural quartz) before and after heat treatment were evaluated from this graph. The measured mechanical properties of all the stones are summarized in Table II.

The elastic modulus of the quartz (E_q) samples was estimated from the reduced modulus (E_s) values obtained directly from the nanoindentation system by using the following formula^[35]:

$$1/E_s = (1 - \sigma_d^2/E_d) + (1 - \sigma_q^2/E_q) \quad [1]$$

where σ and E are the Poisson's ratio and elastic modulus, respectively; the subscript d represents the diamond tip of the Berkovich indenter ($E_d = 1141$ GPa and $\sigma_d = 0.0741$);^[36] and q stands for the quartz sample. Basically, the Oliver–Pharr analysis was adopted for the

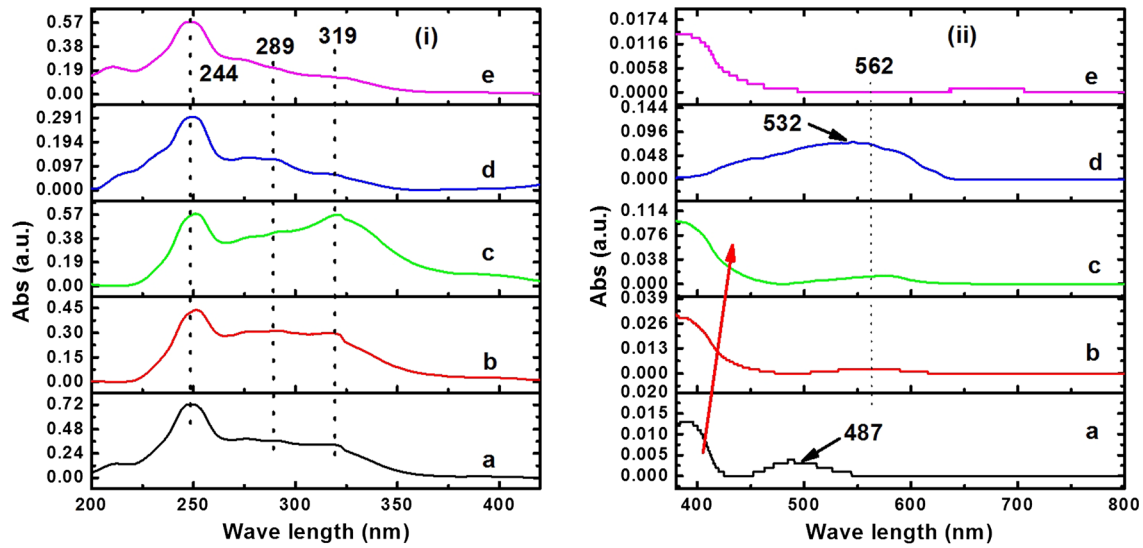


Fig. 4—Comparative UV-Vis-DRS spectra of natural quartz sample before and after heat treatment—(i) full spectra and (ii) spectra in the range of 40 to 800 nm: (a) As-received, (b) heat treated without additive, (c) with Co_3O_4 in vacuum, (d) with Co_3O_4 treatment in open atmosphere, and (e) after Cu_2O treatment.

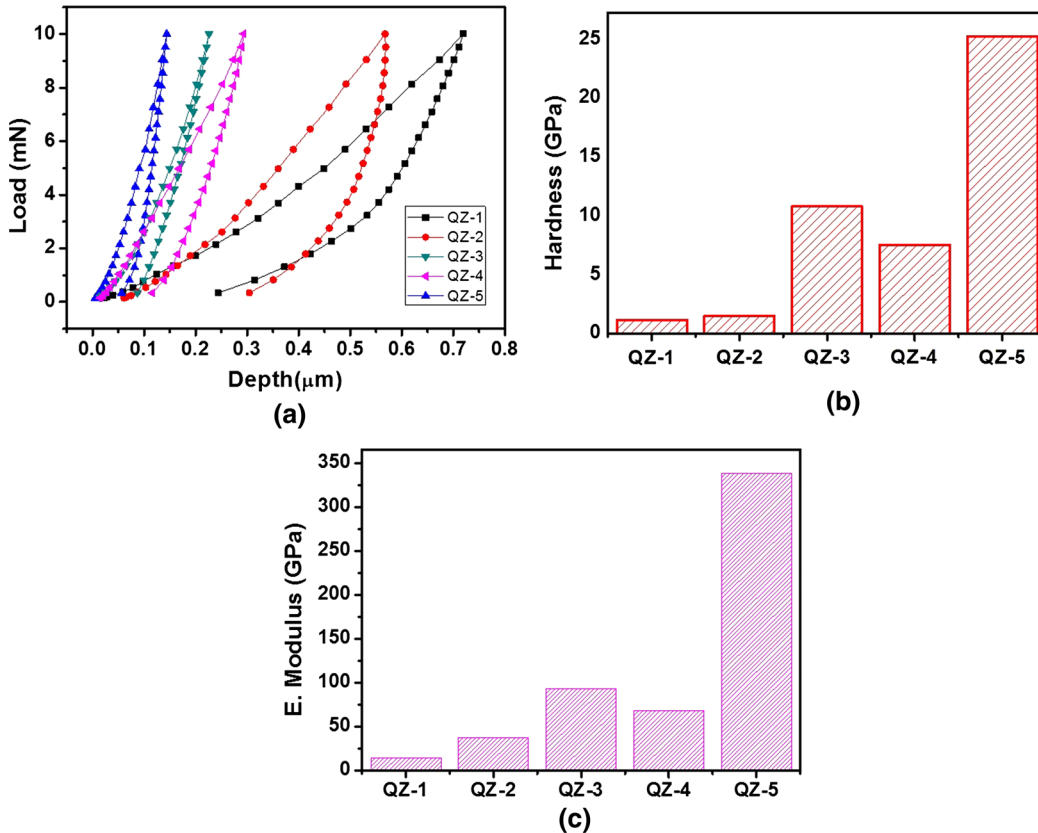
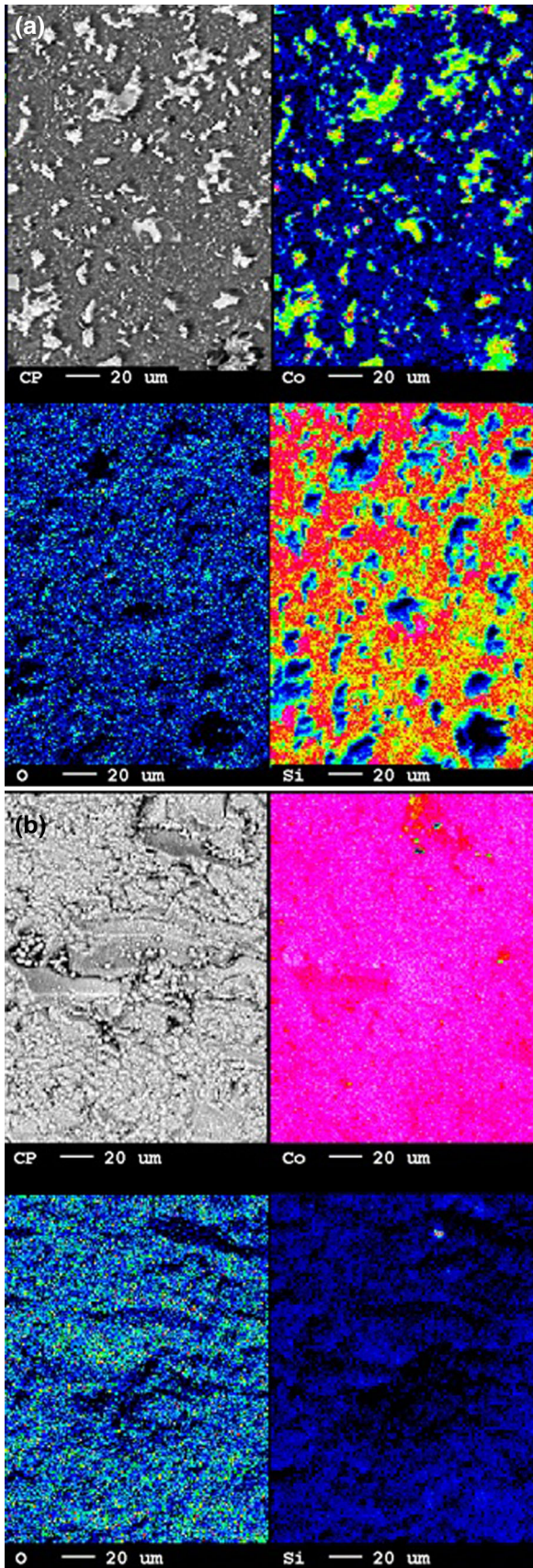


Fig. 5—Nanoindentation values of natural quartz sample before and after heat treatment: (a) load-depth profile, (b) histogram of the hardness value, (c) histogram of the elastic modulus.

estimation of the Young's modulus and hardness values from the load-displacement curve.^[37,38]

It can be seen from Table II that the As-received sample (QZ-1) after acid clean exhibits the lowest value

of both H and E (1.17 and 14.7 GPa, respectively). A marginal increase in the higher H and E values (1.51 and 37.4 GPa) was observed for the heat-treated (QZ-2) sample without any additive. This hardness value is



◀ Fig. 6—(a) EPMA compositional mapping of the surface of the Co_3O_4 vacuum-treated sample. (b) EPMA compositional mapping of the surface of the Co_3O_4 open atmosphere-treated sample.

Table II. Comparison of the Hardness and Elastic Modulus Value of all the Samples

Sample name	H (GPa)	E (GPa)
QZ-1	1.17	14.7
QZ-2	1.51	37.43
QZ-3	10.80	93.07
QZ-4	7.54	67.94
QZ-5	25.26	338.60

found to be very low from the hardness of quartz reported in the literature.^[39,40] When the sample was heat treated in vacuum with a metal oxide additive (sample QZ-3), the H and E values increased to 10.8 and 93.07 GPa, respectively. Slightly lower H and E values (7.54 and 67.94, respectively) were found for the sample heat treated in open air atmosphere (QZ-4). A similar type of result, which is quite comparable to our results, was reported by Broz *et al.*^[39] Thus, when heat treating the quartz with Co_3O_4 in vacuum and open atmosphere, the hardness reaches a value that is close to orthoclase and quartz. However, a significant change in the H and E values (25.26 and 338.6 GPa) was observed for the sample heat treated with copper oxide in open atmosphere. As observed from XRD (Figure 2), the highly crystalline Cu_4O_3 , in combination with the $\text{Cu}_6\text{Si}_6\text{O}_{18}$ phases, that is formed after heat treatment in QZ-5 may be responsible for the higher hardness of the material. Also, as reported in the literature,^[41] the elastic constant of the material depends on the density of the material. Comparing the densities of the As-received and treated samples, changes in densities by 11, 8, and 5 pct of the QZ-5, QZ-4, and QZ-3 samples, respectively, with respect to the QZ-1 sample (shown in Table I) were observed. We also calculated the plasticity index parameter (H/E). This parameter differentiates between the elastic and plastic behaviors of the material. Out of the preceding three heat-treated samples, sample QZ-3 shows the highest value of H/E . Additionally, as reported by Musil and Jirout,^[42] the resistance of the film to plastic deformation is directly related to H^3/E^2 . This relation well suits the oxide carbide and nitride hard thin films. Musil and Jirout also interpreted that the H^3/E^2 term is directly related to the H (hardness of the film). This variation shows parabolic response when plotted against the hardness. In this case, the H^3/E^2 values for QZ-3, 4, and 5 are 0.145, 0.0928, and 0.1405, respectively, in comparison to the QZ-1 and 2 values found to be 0.007 and 0.0024, respectively. This value is highest for the QZ-3 sample. Thus, it implies that heat treatment with cobalt oxide in vacuum forms a shallow cobalt oxide-diffused surface on quartz, which is highly resistant to plastic deformation. The increase in the diffused oxide concentration and formation of the

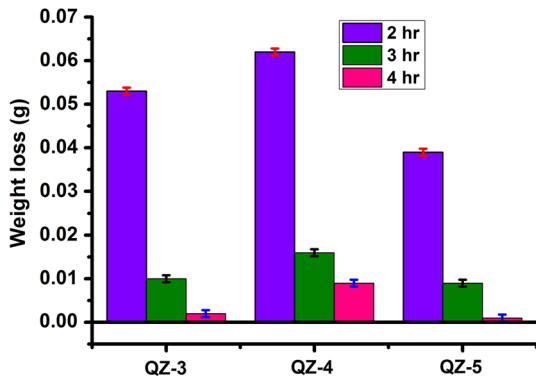


Fig. 7—Weight loss of the metal oxide-treated quartz samples (QZ-3, QZ-4, and QZ-5) in 0.1 N HCl for different times. Blue for 2-h, green for 3-h, and pink for 4-h treatment.

thicker layer improves the chances for plastic deformation. Therefore, treating the transparent quartz with metal oxide additive not only enhances the color but also forms a hard, protective coating on the surface, which improves its aesthetic value to a gemstone grade. It may also be inferred that the metal oxides eliminate the typical vacancies by diffusing in and increasing the adhesivity between the content.

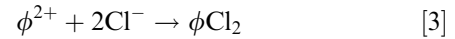
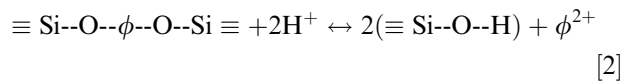
H. EPMA Analysis

The electron micrographs of the Co_3O_4 vacuum and open air heat-treated samples are shown in Figures 6(a) and (b), respectively. The composition map showing the pixel distribution of cobalt in silicon oxide base is worth recording. It may be noted that, in the vacuum-treated sample (Figure 6(a)), irregular clusters of Co are observed in the grain boundary region of quartz. This indicates that Co is not uniformly diffused on the quartz surface. In contrast, in open air thermal treatment (Figure 6(b)), the surface features of quartz show a difference. The Co is uniformly present all over the surface throughout the Si-O base. This finding means that, after open air heat treatment with metal oxide additive, the surface of the sample is covered by a cobalt oxide layer (white spot region) where surface diffusion is less, which is clearly evident from the XRD and Raman data. Thus, this EPMA X-ray mapping completely differentiates the surface elemental content of the two samples and their co-relative change in surface color appearance. Hence, treating the Co_3O_4 in vacuum atmosphere promotes the diffusion of the Co ions at the defect and grain boundary sites, which changes the surface color from transparent to sky blue. However, treating the quartz in open air resulted in the formation of the Co_3O_4 -rich coating on the surface of the quartz. This coating contains a higher concentration of cobalt ions, which results in the deep sky bluish surface coloration.

I. Durability Study

The chemical stability of quartz determines its applications in different fields, especially in gemology; therefore, durability study is of considerable practical importance. Acidic environments effectively remove

the modifiers and leave behind a silica-rich layer on the quartz surface. In this study, the reaction of 0.1 N HCl with the metal oxide-treated quartz samples was examined. When quartz samples (QZ-3, 4, and 5) come in contact with hydrochloric acid solution, H^+ ions from etchant solution replace the diffused cations on the quartz surface. Basically, it follows the reaction as^[43]



where ϕ stands for Co^{2+} and Cu^{2+} ions. Initially, the reaction occurs (Reaction [2]) with the preferential leaching of metal ions from the quartz surface, corresponding to the initial removal of metal ions from the lattice and subsequent formation of the passive film. This passive film is less stable in the presence of Cl^- ions. Thus, the presence of dissociated Cl^- ions enhances the rate of reaction. Additionally, the presence of Cl^- ions enhances the redox potential, creating a more oxidizing condition by following Reaction [3]. From the preceding reactions, the diffused cation depleted region matrix in the initial reaction (Reaction [2]) is formed. Water molecules can easily penetrate in and attack the quartz matrix. Thus, the amount of the diffusing ions in the quartz matrix significantly affects the durability of the quartz.^[44]

On the other hand, the ionic radii of the cations allow them to occupy the octahedral sites in the quartz (instead of tetrahedral ones), in which the bonds between ions and the surrounding oxygen are the weakest links as compared to $\phi\text{-Si-O}$ or $\text{Si-}\phi\text{-O}$ bonds. The stronger the cation and oxygen bond, the higher is the chemical resistance of the treated quartz. As observed from the XRD and nanoindentation data, the harder and high crystalline phase on the surface of the quartz by the treatment of copper oxide resulted in greater chemical durability. Also, the presence of a higher number density of Co^{2+} ions with thicker coating in open air treatment with cobalt oxide resulted in lower chemical durability. Additionally, the effect of treatment time and the factors affecting the chemical durability were studied. Figure 7 shows the histogram of weight loss of QZ-3, QZ-4, and QZ-5 samples in different times. The histogram in Figure 7 clearly indicates that the weight loss is maximum for the cobalt oxide open air-treated sample (QZ-4) and minimum for the copper oxide-treated sample (QZ-5) treated for 2 hours. A similar trend was also observed for the 3-hour treated samples. However, extending this exposure time to 4 hours did not show any significant loss. After this test was performed, the appearance of these stones was dramatically changed. Nevertheless, because the modifiers were removed only to a limited depth, their overall feature appears better than the untreated one.

The preceding results indicated that the Cu_2O -treated (QZ-5) sample shows a very low rate of leaching in comparison to the cobalt oxide-treated samples (QZ-3 and QZ-4). The cobalt oxide-treated quartz sample in

vacuum showed relatively low leaching yield in comparison to the open air-treated cobalt oxide-treated sample. This finding also indicated that the metallic ion diffusion and attachment to the quartz matrix are quite superior in the case of vacuum atmosphere. Additionally, the indentation result in correlation with the preceding findings confirmed that this enhanced strength of the materials achieved by the diffusion of the metallic ion into the quartz matrix increased the cross-link bond strength between the cations and oxygen. Similar results were also observed by other groups,^[44,45] which reported that the glass containing rare earth oxides exhibits higher chemical stability.

IV. CONCLUSIONS

The main findings of this study can be summarized as follows:

1. Changes in structural, physical, and chemical properties of the natural quartz were investigated by introducing Co₃O₄ in different atmospheres and Cu₂O in open atmosphere.
2. Elemental analysis confirms the presence of impurities such as Fe, Al, Ti, and Zn in the natural quartz samples, which modifies the optical absorption.
3. Both the hardness and specific gravity values of quartz increased from 1.1 to 25.61 GPa and 2.66 to 3.01 g/cm³, respectively, by the diffusion of the metal oxide. The greater strength of the cross-links between the cation and oxygen atoms results in the increase of structural rigidity of the metal oxide-containing quartz. Structural investigation by XRD and Raman spectroscopy revealed phase changes on the surface after heat treatment with metal oxide additives. Diffusing environments had a substantial effect on the change of surface properties.
4. EPMA images confirmed that, with heat treatment in vacuum atmosphere, cobalt ions diffuse more inside the quartz matrix, whereas in ambient heat treatment, a coating forms on the surface of the quartz.
5. The chemical durability of the thermal-diffused quartz as a function of time in an aqueous solution was compared. The Cu₂O-treated quartz sample was found to exhibit better stability to chemical hars environment.

ACKNOWLEDGMENTS

We thank the Council of Scientific and Industrial Research (Grant No. ESC-0206) for providing the funding to pursue this work. We also thank Mrs. Swatirupa Pani and Mr. Shubhra Bajpai for their help with the EPMA and microindentation measurements, respectively.

REFERENCES

1. T. Götte, T. Pettke, K. Ramseyer, M. Koch-Müller, and J. Mullis: *Am. Mineral.*, 2011, vol. 96, pp. 802–13.

2. I.K. Bailiff, L. Botter-Jensen, V. Correcher, A. Delgado, H.Y. Göksu, H. Jungner, and S.A. Petrov: *Radiat. Meas.*, 2000, vol. 32, pp. 609–13.
3. A.N. Yazici, M. Bedir, H. Bozkurt, and H. Bozkurt: *Nucl. Instrum. Methods Phys. Res. Sect. B: Beam Interact. Mater. Atoms*, 2008, vol. 266, pp. 613–20.
4. N. Porat, T. Levi, and R. Weinberger: *Israel Quat. Geochronol.*, 2007, vol. 2, pp. 272–77.
5. F. Preusser, M.L. Chithambo, T. Götte, M. Martini, K. Ramseyer, E.J. Sendezer, G.J. Susino, and A.G. Wintle: *Earth-Sci. Rev.*, 2009, vol. 97, pp. 184–214.
6. G. Adamiec: *Radiat. Meas.*, 2005, vol. 39, pp. 105–10.
7. K. Xi, Y. Cao, J. Jahren, R. Zhu, K. Bjørlykke, X. Zhang, L. Cai, and H. Hellevang: *Mar. Pet. Geol.*, 2015, vol. 66, pp. 748–63.
8. Y. Ogimoto, R. Selyanchyn, N. Takahara, S. Wakamatsu, and S.-W. Lee: *Sens. Actuators B*, 2015, vol. 215, pp. 428–36.
9. J. Zhu, S. Huang, J. Ye, X. Zhang, and G. Liu: *Sens. Actuators A*, 2015, vol. 229, pp. 141–46.
10. S. Toyoda: *Quat. Geochronol.*, 2015, vol. 30, pp. 498–505.
11. C. Schmidt, S. Kreutzer, R. DeWitt, and M. Fuchs: *Quat. Geochronol.*, 2015, vol. 27, pp. 66–77.
12. H. Wu, L. Dong, W. Ren, W. Yin, W. Ma, L. Zhang, S. Jia, and F.K. Tittel: *Sens. Actuators B*, 2015, vol. 206, pp. 364–37.
13. L. Botaya, J. Otero, L. González, X. Coromina, G. Gomila, M. Puig-Vidal, and A.C. Caballero: *Sens. Actuators A*, 2015, vol. 232, pp. 259–66.
14. A. Muller, M. Wiedenbeck, A.M. Van Den Kerkhof, A. Kronz, and K. Simon: *Eur. J. Mineral.*, 2003, vol. 15, pp. 747–63.
15. A.I. Serebrennikov, A.A. Valter, R.I. Mashkovtsev, and M.Y. Scherbakova: *Phys. Chem. Miner.*, 1982, vol. 8, pp. 153–57.
16. P.C. Schultz: *J. Am. Ceram. Soc.*, 1974, vol. 57, pp. 309–13.
17. N. Song, Y. Wang, Y. Hu, Y. Huang, W. Li, S. Huang, and X. Hao: *Appl. Phys. Lett.*, 2014, vol. 104, p. 092103.
18. Y.J. Zhao, Z.G. Yin, X.W. Zhang, Z. Fu, B.J. Sun, J.X. Wang, and J.L. Wu: *ACS Appl. Mater. Interfaces*, 2014, vol. 6, pp. 2639–46.
19. S.C. Moulzolf, L.J. LeGore, and R.J. Lad: *Thin Solid Films*, 2001, vol. 400, pp. 56–63.
20. A. Sehirlioglu, D.A. Payne, and P. Han: *Phys. Rev. B*, 2005, vol. 72, p. 214110.
21. K.J. Kingma and R.J. Hemiley: *Am. Mineral.*, 1994, vol. 79, pp. 269–73.
22. C.C. Lin: *Phys. Chem. Miner.*, 2001, vol. 28, pp. 249–57.
23. M. Bouchard and A. Gambardella: *J. Raman Spectrosc.*, 2010, vol. 41, pp. 1477–85.
24. L. Debbichi, M.C. Marco de Lucas, J.F. Pierson, and P. Krüger: *J. Phys. Chem. C*, 2012, vol. 116, pp. 10232–37.
25. D.A. McKeown, C.C. Kim, and M.I. Bell: *Phys. Chem. Miner.*, 1995, vol. 22, pp. 137–44.
26. C.D. Marshall, J.A. Speth, and S.A. Payne: *J. Non-Cryst. Solids*, 1997, vol. 212, pp. 59–73.
27. A. Oliver, J.C. Cheang-Wong, A. Crespo, J.M. Hernández, C. Solís, E. Muñoz, R. Espejel-Morales, and J. Siejka: *Appl. Phys. Lett.*, 1998, vol. 73, p. 14.
28. L.B.F. de Souza, P.L. Guzzo, and H.J. Khoury: *J. Lumin.*, 2010, vol. 130, pp. 1551–56.
29. J. Gotze, M. Plotze, and D. Habermann: *Miner. Petrol.*, 2001, vol. 71, pp. 225–50.
30. M. Martini, A. Paleari, G. Spinolo, and A. Vedda: *Phys. Rev. B*, 1995, vol. 52, p. 138.
31. I. Simkiene, A. Reza, A. Kindurys, V. Bukauskas, J. Babonas, R. Szymczak, P. Aleshkevych, M. Franckevicius, and R. Vaisnoras: *Lith. J. Phys.*, 2010, vol. 50, pp. 7–15.
32. S. Muller, M. Zhou, Q. Li, and C. Ronning: *Nanotechnology*, 2009, vol. 20, p. 135704.
33. R. He, B. Tang, C. Ton-That, M. Phillips, and T. Tsuzuki: *J. Nanopart. Res.*, 2013, vol. 15, p. 2030.
34. A. Bautista-Hernández, U. Pal, L. Rodríguez-Fernández, and J.C. Cheang-Wong: *Superficies y Vacío*, 1999, vol. 9, pp. 296–99.
35. A.C.F. Cripps: *Nanoindentation*, Springer, New York, NY, 2004.
36. S. Bajpai, A. Gupta, S.K. Pradhan, T. Mandal, and K. Balani: *JOM–J. Miner. Met. Mater. Soc.*, 2014, vol. 66, pp. 2095–2107.
37. W.C. Oliver and G.M. Pharr: *J. Mater. Res.*, 1992, vol. 7, pp. 1564–83.

38. G.M. Pharr: *Mater. Sci. Eng. A*, 1998, vol. 253, pp. 151–59.
39. M.E. Broz, R.F. Cook, and D.L. Whitney: *Am. Mineral.*, 2006, vol. 91, pp. 135–42.
40. W. Zhu, J.J. Hughes, N. Bicanic, and C.J. Pearce: *Mater. Charact.*, 2007, vol. 58, pp. 1189–98.
41. W. Pabst and E. Gregorová: *Ceram.-Silik.*, 2013, vol. 57, pp. 167–84.
42. J. Musil and M. Jirout: *Surf. Coat. Technol.*, 2007, vol. 201, pp. 5148–52.
43. R.A. Rahimi, S.K. Sadrnezhad, and G. Raisali: *J. Non-Cryst. Solids*, 2009, vol. 355, pp. 169–74.
44. E.A. Mahdy and S. Ibrahim: *J. Mol. Struct.*, 2012, vol. 1027, pp. 81–86.
45. K. Singh, I. Bala, and V. Kumar: *Ceram. Int.*, 2009, vol. 35, pp. 3401–06.